Iron(IV) Alkyl Hydrazido Complexes: Electronic Structure, Fe–C Bond Homolysis, and N–C Bond Forming Migration Reactions

*Samuel M. Bhutto, Sean F. McWilliams, Reagan X. Hooper, Brandon Q. Mercado, Patrick L. Holland**

Department of Chemistry, Yale University, New Haven, Connecticut

* email: patrick.holland@yale.edu

Abstract

High-valent iron-alkyl complexes are rare, as they are typically prone to Fe–C bond homolysis. We show here an unusual way to access formally iron(IV) alkyl complexes through double silylation of iron(I) alkyl dinitrogen complexes to form an $NNSi_2$ group. When the alkyl group is trimethylsilylmethyl, the formally iron(IV) compound is stable at room temperature. Spectroscopically validated computations show that the disilylhydrazido(2–) ligand stabilizes the formal iron(IV) oxidation state through a strongly covalent Fe–N π-interaction, in which one π-bond fits an "inverted field" description. This means that the two bonding electrons are localized on the metal and not the ligand, and an iron(II) resonance structure is a significant contributor as with the phenyl analogue. However, in contrast to the phenyl analogue which has an $S = 1$ ground state, the ground state of the alkyl complex is S = 2, and this places one electron in the π* orbital and weakens the Fe–N bonding, leading to longer Fe–N bonds. The reactivity of these hydrazido(2–) complexes has an interesting dependence on the specific alkyl group. When the alkyl group is methyl, the formally iron(IV) species undergoes migration of the carbon-based ligand to the $NNSi_2$ group to form a new N–C bond, followed by an intriguing isomerization of the hydrazido ligand. This reactivity is not observed with the bulkier trimethylsilylmethyl complex. When the alkyl group is benzyl, yet another reactivity pathway is evident: the Fe–C bond homolyzes to give a three-coordinate iron(III) complex with a hydrazido(2–) ligand. DFT calculations are used to explain the differences between the behavior with the different alkyl groups. Overall, these formally iron(IV) compounds display a diverse set of reaction pathways associated with the specific alkyl groups.

Introduction

The isolation of iron(IV) compounds has been dominated by oxo, nitrido, and imido complexes, because the π-bonds help to stabilize the high oxidation state.[1-13] However, reports of organometallic iron(IV) alkyl complexes are rare.[14-19] This is likely because high-valent iron alkyl species are prone to Fe–C bond homolysis to give an iron(III) complex plus the corresponding alkyl radical,[15, 17] exemplified by the well-documented reactivity of alkyliron porphyrin complexes (Figure 1a).[20-25] In contrast, Wolczanski and coworkers reported that NHC-supported alkyliron(IV) complexes could be generated by addition of AdN_3 to an iron(II) dialkyl complex, and these complexes were more resistant to Fe–C homolysis. Instead, they underwent alkyl group migration to the imido ligand to produce the corresponding amidoiron(II) complexes (Figure 1b).[16] To our knowledge, this is the only well-characterized example of alkyl migration from a transition metal to a M=NR group, though this step may be involved in some reactions where a metal-alkyl undergoes amination by addition of an azide.[26-27] Meyer has also reported insertion of a coordinated NHC ligand into the Co–N bond of a Co=NR compound.[28]

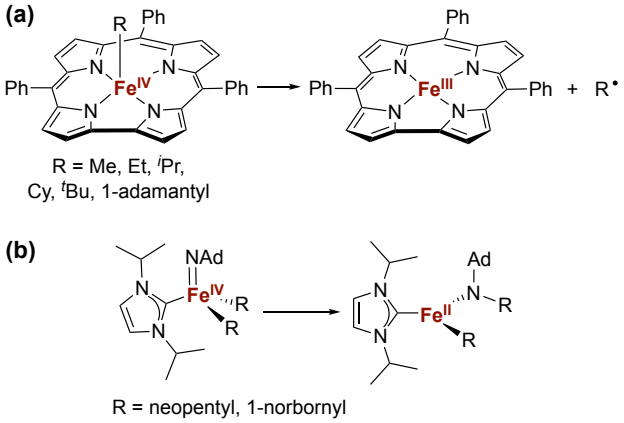

Figure 1. Examples of previously reported iron(IV) alkyl complexes and degradation pathways.

Our research in this area emerged from the study of formally iron(IV) aryl species that undergo migration of the aryl group to the Fe-bound NNR_2 group (Scheme 1).[29] The reaction sequence of interest starts with the reaction of iron(I) aryl N_2 complexes (**1-N_2**) with two equivalents of Me_3SiX (X = Br, I, OTf; OTf = trifluoromethanesulfonate) and one equivalent of reducing agent. This gives a double silylation at the distal N atom and net three-electron oxidation at the metal, resulting in a formally iron(IV) complex with aryl and hydrazido(2–) ligands (**2**). It is this complex that can perform the migration of the aryl group from Fe to the proximal N atom to form a new N–C bond in a hydrazido product (**3**). Since the phenyl group in **1** can be derived from the C–H activation of benzene, **t**his migration is exciting because it combines two abundant starting materials, N_2 and benzene, into a cross-coupled product.

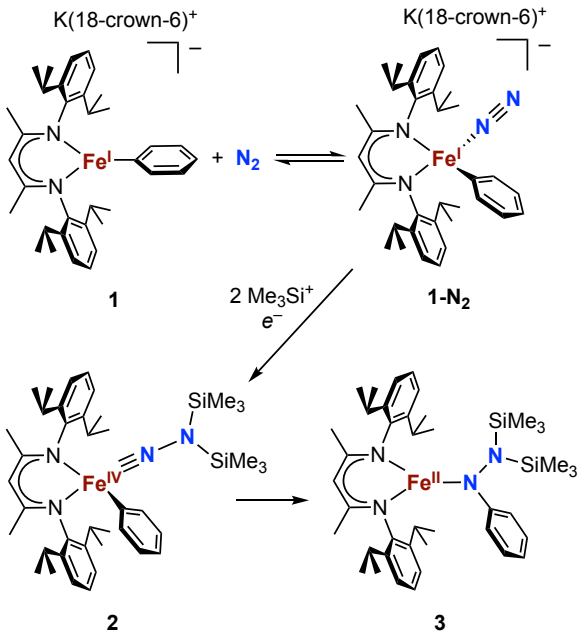

Scheme 1. Formation of a formally iron(IV) hydrazido(2–) complex from N_2, and subsequent migratory insertion of the aryl ligand to the N-containing group.

So far, the reported migrations of hydrocarbyl groups from Fe to N have been limited to iron-*aryl* complexes. Since N_2 binding has been reported in a β-diketiminatoiron(I) *alkyl* complex

as well,[30] we hypothesized that iron(IV) *alkyl* hydrazido(2–) complexes might undergo alkyl migration by analogy to the aryl migrations. Previously, Peters had described *hydride* migration to a hydrazido(2–) ligand at a formally iron(IV) center, suggesting that migration chemistry may not be limited to aryl groups.[31] Herein, we describe a series of iron(I) alkyl complexes that bind N_2 at low temperatures and their reactivities upon N_2 silylation, including the characterization of the first formally iron(IV) alkyl hydrazido(2–) complex that is stable at room temperature. In some cases, N–C bond formation occurs but in others homolysis causes loss of the alkyl group without N–C bond formation. Density functional theory (DFT) calculations give insight into the competition between Fe–C bond homolysis and alkyl migration pathways.

Results and Discussion

The alkyl chemistry described here starts from the high-spin iron(II) alkyl complexes **4a-4c**, which are stable despite a 12-electron configuration at iron.[30, 32-34] Previous work has shown that an analogous β-diketiminatoiron(II) alkyl complex can be reduced to the iron(I) oxidation state, and then when this iron(I) complex is cooled under N_2 it binds to the iron center.[29-30] Accordingly, we prepared the iron(I) complexes **5a-5c** by reduction of the corresponding iron(II) alkyl complexes with KC_8 in the presence of 18-crown-6, and isolated them in *ca.* 80% yield (Scheme 2). Complex **5c** was isolated and fully characterized previously.[30] Crystals of the new complexes **5a** and **5b**, grown from concentrated solutions of THF layered with hexanes stored at –35 °C overnight, yielded X-ray crystallographic structures (Figure 2). The average Fe–N_{nacnac} bond lengths of **5a** (1.928(5) Å) and **5b** (1.918(3) Å) are equivalent to that in **5c** (1.922(4) Å). The Fe–C bond length of **5b** (2.063(4) Å) is longer than that in the starting iron(II) complex **4b** (2.041(2) Å),[34] consistent with the lower oxidation state, while the Fe–C bond lengths of **5a** and

4a are equivalent (**5a**, ave. 2.015(2) Å; **4a**, 2.022(2) Å).[34] Similarly, the Mössbauer parameters of **5a** (δ = 0.44 mm s^{-1}, $|\Delta E_Q|$ = 1.90 mm s^{-1}) and **5b** (δ = 0.27 mm s^{-1}, $|\Delta E_Q|$ = 1.75 mm s^{-1}) are similar to those reported for high-spin **5c** (δ = 0.38 mm s^{-1}, $|\Delta E_Q|$ = 2.06 mm s^{-1}).[35] Consistent with this assignment, solution Evans method studies indicate high-spin ground states for **5a** (μ_{eff} = 4.3(1) μ_B) and **5b** (μ_{eff} = 4.3(1) μ_B).

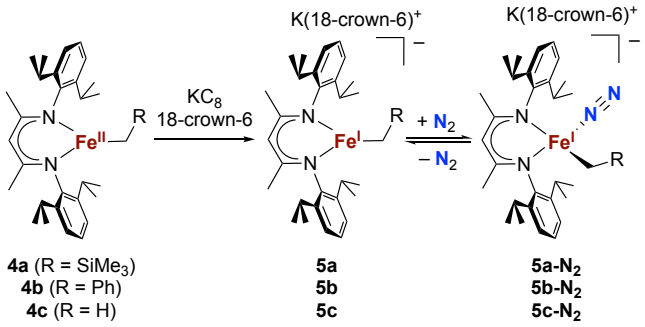

Scheme 2. Synthesis of iron(I) alkyl complexes **5a-5c** and reversible N_2 binding.

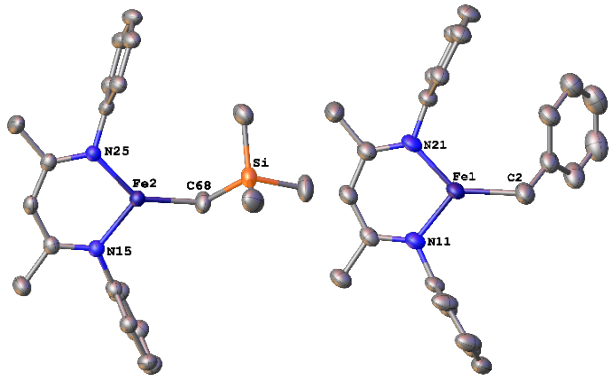

Figure 2. ORTEP diagrams of complexes **5a** (left) and **5b** (right) with thermal ellipsoids shown at 50% probability. H atoms, ^{i}Pr groups, and K(18-crown-6)(THF)$_2^+$ cations are omitted for clarity, as well as a molecule of THF in the asymmetric unit of **5a**.

We then investigated the N_2 binding capabilities of the iron(I) alkyl complexes at low temperature. Freezing solutions of **5a-5c** in THF under an atmosphere of N_2 led to a color change

of the solutions from green to magenta, and thawing the solutions gave back the original green color. These color changes were not observed when freezing solutions under an atmosphere of Ar. Van't Hoff analysis of the variable-temperature ^{1}H NMR (**5a** and **5b**) and UV-vis (**5c**) spectra gave the thermodynamic parameters shown in Table 3.1. The negative enthalpy and entropy for each complex indicate N_2 binding at lower temperatures, likely in an end-on fashion as proposed in the analogous iron β-diketiminate systems mentioned above.[29-30]

Table 1. Results from van't Hoff analysis of variable-temperature spectroscopic measurements of **5a**-**5c** under N_2.

	ΔH (kcal mol^{-1})	ΔS (e.u.)
5a	–8.8(6)	–52(3)
5b	–9.5(6)	–57(2)
5c	–4.3(7)	–33(3)

Next we explored the silylation of the N_2-bound complexes to form formally iron(IV) complexes (Scheme 3). Addition of the bis(silyl) reagent **6** to a mixture of **5a-N$_2$** and K(18-crown-6)($C_{10}H_8$) (used as an external reductant) in Et_2O at –116 °C led to an immediate color change from magenta to brown. The ^{1}H NMR spectrum of the crude reaction mixture showed the formation of a new C_s symmetric complex in 73% spectroscopic yield. Cooling a concentrated hexamethyldisiloxane (HMDSO) solution at –35 °C overnight led to the isolation of brown crystals in 32% yield, which were identified by X-ray diffraction as the formally iron(IV) complex **7a** (Figure 3, top). The N–N bond length is 1.326(3) Å, between the values for a N–N single bond (1.45 Å) and double bond (1.25 Å) in the corresponding free organic N_2H_x compounds, and is comparable to those in other four-coordinate iron hydrazido(2–) complexes as well as the

previously isolated formally iron(IV) phenyl complex **2** (1.340(4) Å).[36-38] However, the bond lengths to iron in **7a** are significantly different than those in **2**. The Fe–N_{hyd} bond length (1.749(2) Å) and average Fe–N_{nacnac} bond length (2.051(1) Å) in **7a** are ~0.08 Å longer than those in **2** (1.673(3) and 1.970(2) Å, respectively). Additionally, the iron center in **7a** adopts a distorted tetrahedral geometry (τ_4 = 0.88) compared to distorted trigonal pyramidal in **2** (τ_4 = 0.75).

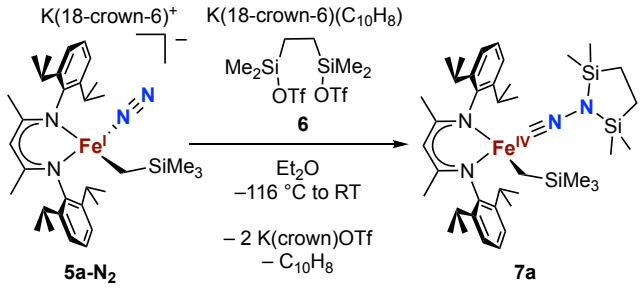

Scheme 3. Synthesis of the formally iron(IV) complex **7a**.

The zero-field Mössbauer spectrum of **7a** showed a doublet with an isomer shift of δ = 0.33 mm s^{-1}, which is much higher than δ = 0.17 mm s^{-1} in **2** (Figure 3, bottom). The higher isomer shift in **7a** may indicate that the complex has a different ground spin state, and the longer bonds in **7a** noted above suggest the higher spin state of S = 2. Furthermore, the bond distances to the iron center in **7a** closely resemble those observed in a DFT model of **2** in an S = 2 state.[38] Finally, solution magnetic susceptibility measurement gave μ_{eff} = 5.0(2) μ_B, which confirms the high-spin ground state.

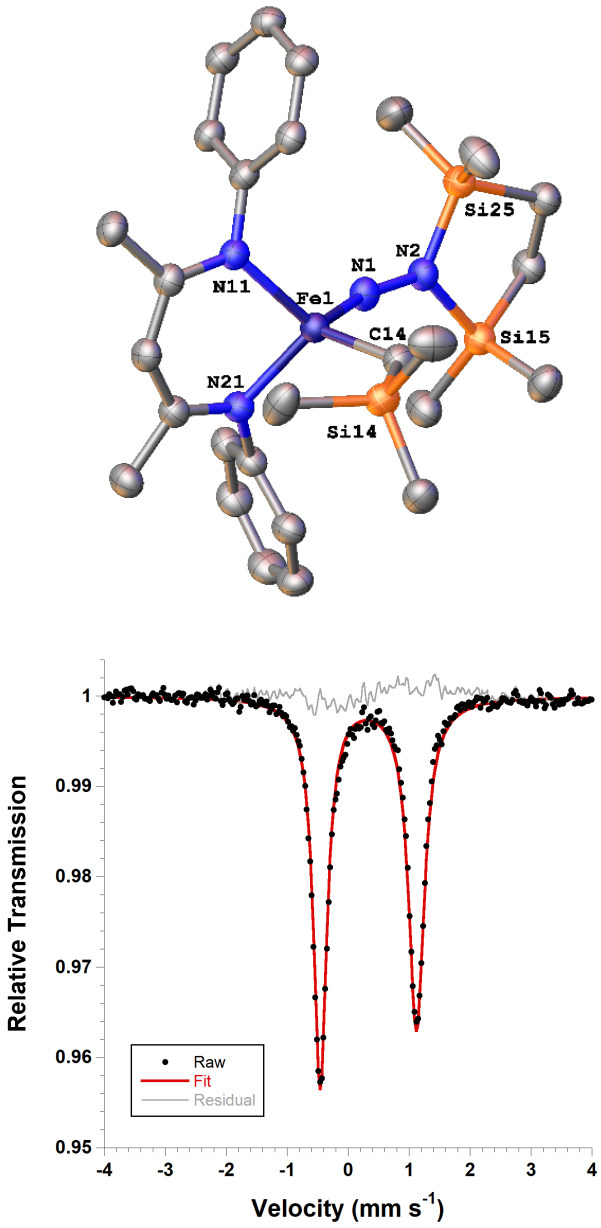

Figure 3. (Top) ORTEP diagram of **7a** with thermal ellipsoids shown at 50% probability, with H atoms and ^{i}Pr groups omitted for clarity. (Bottom) Solid state zero-field Mössbauer spectrum of **7a** at 80 K.

DFT calculations were performed for greater insight into the electronic structure of **7a**. The geometry of **7a** in an $S = 2$ ground state was optimized at the B3LYP/def2-TZVP level. The quasi-restricted orbitals (QROs) of this optimized structure of **7a** are shown in Figure 4, with the z axis

chosen to be along the Fe–hydrazido(2–) bond. The Fe–N_{hyd} π bonding interaction involving the Fe d_{yz} orbital has more hydrazido than iron character, typical of a normal π bond. The π bonding interaction involving the Fe d_{xz} orbital, however, has greater Fe character, and the antibonding interaction has more ligand character. This "inverted ligand field" suggests that the formal oxidation state of 4+ may not accurately represent the physical oxidation state at iron in **7a**.[39] Since two of the electrons that belong to the ligand in formal oxidation state calculation are actually polarized toward the metal, it suggests a resonance structure with iron(II) and a neutral isodiazene ligand. The formal bond order of the Fe–N_{hyd} bond is 2.5, as the Fe d_{yz} π* orbital is singly occupied. This is consistent with the longer Fe–N_{hyd} bond distance in **7a** compared with that of **2**, which has an $S = 1$ ground state and a formal Fe–N_{hyd} bond order of 3.

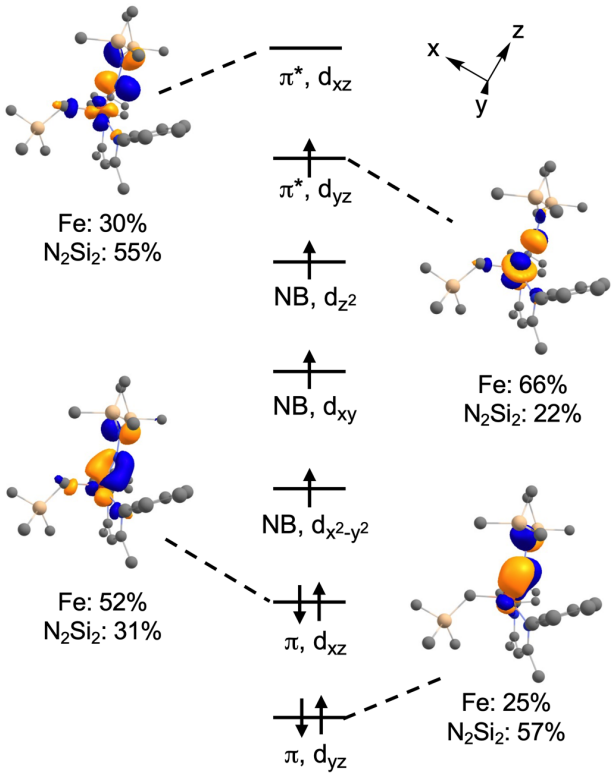

Figure 4. Qualitative molecular orbital diagram showing the QROs of **7a** ($S = 2$) with selected QRO plots shown at an isovalue of 0.05 au.

We then turned to the solution behavior of **7a** in comparison to **2**. Complex **7a** was significantly more stable in solution, showing only about 25% decomposition after 4 days in C_6D_6 solution at room temperature, whereas **2** is completely converted within a couple of hours at room temperature. Heating a C_6D_6 solution of **7a** at 80 °C for 2 hours led to the complete consumption of the formally iron(IV) species. However, the product was not alkyl migration (in analogy to **2**) but rather formation of the iron(II) alkyl complex **4a** (24%) and other species as quantified by ^{1}H NMR spectroscopy (see SI for more details). We propose that complex **4a** may result from the decomposition of **7a** via homolytic cleavage of both N–Si bonds of the hydrazido(2–) unit and N_2 dissociation from the resulting iron(II) center. A related N–Si bond cleavage has been observed from an iron silyldiazenido complex by Ashley.[40]

We also explored the silylation reactivity of the other iron(I) alkyl complexes. Unlike the silylation reaction of **5a-N$_2$**, the use of K(18-crown-6)($C_{10}H_8$) as an external reductant in the reaction of the iron(I) benzyl complex **5b-N$_2$** and the silyl triflate **6** led to an intractable mixture of unidentified species. However, it has previously been shown in the synthesis of a related aryl diazenido species that the starting iron(I) aryl complex can provide the necessary electron equivalent in the reaction (unfortunately limiting the yield of silylated product to a maximum of 50% based on iron).[29] Thus, addition of **6** to a solution of **5b-N$_2$** in Et_2O at –116 °C without an external reductant led to the formation of the oxidized iron(II) product **4b** in 64% spectroscopic yield (quantified by ^{1}H NMR spectroscopy), as well as a new C_{2v} symmetric species **8** in 22% spectroscopic yield (Scheme 4, left). This same species **8** was also identified in the decomposition mixture of **7a** in 27% spectroscopic yield, indicating that it had lost the alkyl group. X-ray diffraction revealed **8** to be an iron(III) hydrazido complex (Figure 5, top). In a route similar to the

one previously used for the synthesis of the trimethylsilyl analogue LFeNN(SiMe$_3$)$_2$ (L = 2,4-bis(2,6-diisopropylphenylimido)pentyl),[41] complex **8** could also be prepared from the reaction of the iron(0)-bis(dinitrogen) complex **9** and 1,2-bis(chlorodimethylsilyl)ethane in 22% isolated yield (Scheme 4, upper right). We propose that **8** may have formed through initial silylation of **5b-N$_2$** to give the formally iron(IV) complex **7b** followed by Fe–C bond homolysis,[17, 25, 42-43] producing a benzyl radical (Scheme 4, bottom). Indeed, trapping experiments, in which the radical scavenger TEMPO (TEMPO = 2,2,6,6-tetramethylpiperidine 1-oxyl) was added to the reaction mixture immediately after silane addition at –116 °C, showed the formation of the TEMPO-benzyl adduct[44] (> 80% ^{1}H NMR spectroscopic yield when K(18-crown-6)(C$_{10}$H$_8$) is added to increase the yield of **7b** formed *in situ*). This mechanism is also consistent with the formation of **8** upon heating solutions of **7a** which would proceed via loss of the corresponding trimethylsilylmethyl radical.

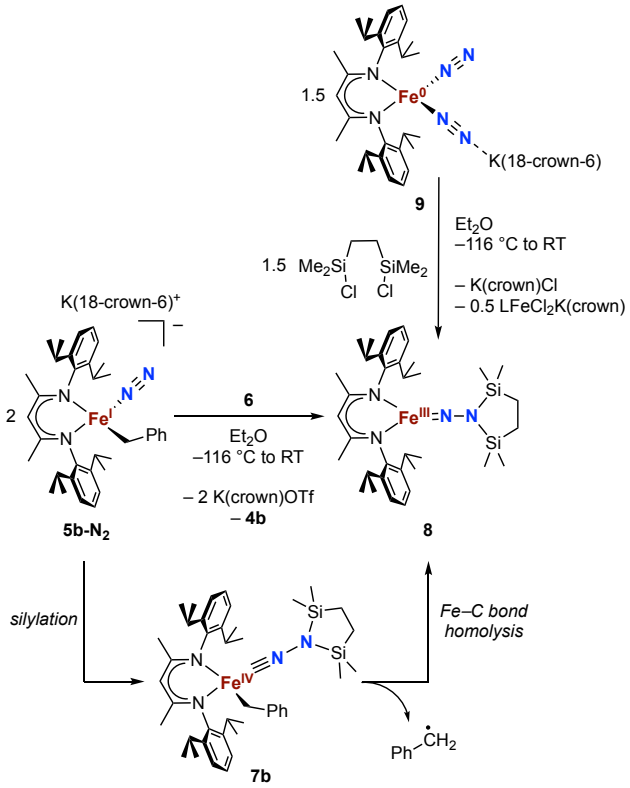

Scheme 4. Syntheses of the iron(III) hydrazido complex **8**, and proposed mechanism of formation from **5b-N$_2$**.

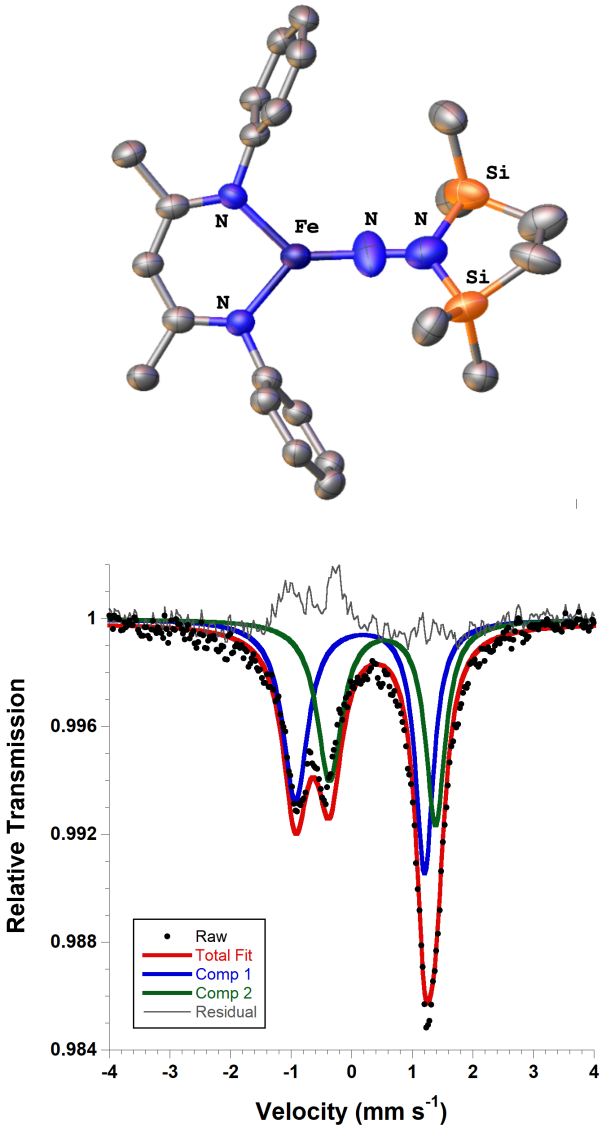

Figure 5. Top: ORTEP diagram of **8** with thermal ellipsoids shown at 50% probability and H atoms and ^{i}Pr groups omitted for clarity; due to apparent disorder in the core, the structure is for connectivity only. Bottom: solid state zero-field Mössbauer spectrum of **8** at 80 K.

Unfortunately, the X-ray crystal structure solution of **8** had a second component in the core that prevents us from deriving reliable metrical parameters, and we were unable to purify samples sufficiently for microanalysis. However, the spectroscopic characterization was intriguing. Like

the previously characterized trimethylsilyl analogue LFeNN($SiMe_3$)$_2$,[45] the solid state Mössbauer spectrum of crystalline **8** collected at 80 K shows two doublets in a 1:1 ratio with isomer shifts of 0.13 and 0.51 mm s^{-1} (Figure 5, bottom). In the previous work, the 1:1 ratio was explained by the presence of two molecules with significantly different bond distances in the crystallographic asymmetric unit. Comparison to calculations (see further) and fitting of magnetic susceptibility data indicated that the two molecules had different spin states (S = 1/2 and S = 3/2).[45] In order to determine whether this might be the case in **8** as well, DFT calculations were carried out to determine the relative energies of the S = 1/2 and S = 3/2 ground state configurations using geometry-optimized structures of **8** (Table 2). Calculations using both the BP86 and B3LYP functionals show a small energy difference between the doublet and quartet states, with the low-spin conformer lower in energy by 9 kcal mol^{-1} with BP86, while B3LYP predicts the high-spin state to be lower by 2 kcal mol^{-1}. This difference in lowest energy calculated spin conformer is to be expected, as hybrid functionals such as B3LYP have been shown to favor higher spin states.[47] These small differences in energy suggest that these spin isomers could indeed be isoenergetic. Importantly, the calculated Mössbauer parameters of the geometry-optimized doublet and quartet DFT models are in excellent agreement with the two signals in the spectrum of **8** (Table 2).[48]

Table 2. Comparison of bond lengths and Mössbauer parameters between the experimental structures of **8** and LFeNN(SiMe$_3$)$_2$ versus DFT computed parameters using BP86 and B3LYP. All computations used the def2-TZVP basis set.

Compound	Functional	Spin state	Fe–N_2 (Å)	Ave. Fe–N_{nacnac} (Å)	Rel. Energy (kcal mol^{-1})	δ (mm s^{-1})	$\|\Delta E_Q\|$ (mm s^{-1})
8	Exp.	1/2				0.13	2.13
		3/2				0.51	1.75
	BP86	1/2	1.627	1.872	0	0.12	2.04
		3/2	1.689	1.911	9	0.48	1.83
	B3LYP	1/2	1.653	1.914	2	0.24	1.76
		3/2	1.731	1.980	0.0	0.67	1.36
LFeNN(SiMe$_3$)$_2$ (ref 41)	Exp.	1/2	1.638(2)	1.924(1)		0.22	1.99
		3/2	1.671(2)	1.948(1)		0.46	1.16
	BP86	1/2	1.628	1.885	0.0	0.14	1.93
		3/2	1.690	1.919	9	0.51	1.72
		5/2	1.774	1.962	31	0.61	3.69
	B3LYP	1/2	1.660	1.924	1		
		3/2	1.725	1.972	0		
		5/2	1.850	2.002	15		

Additionally, the electron paramagnetic resonance (EPR) spectrum of a frozen toluene solution of **8** collected at 5 K shows two spin-active species consistent with an $S = 1/2$ and $S = 3/2$ species (Figure 6, bottom). Simulating the spectrum gives an $S = 1/2$ species with $\boldsymbol{g}$ = [1.80, 1.84, 3.54]. The large anisotropy of g values was similarly observed in the previously reported trimethylsilyl analogue which had $\boldsymbol{g}$ = [1.79, 1.84, 3.61].[45] The small signals with g_{eff} values of 6.21 and 2.32 are reminiscent of a three-coordinate, intermediate-spin (S = 3/2) iron(III) imido complex with the same diketiminate supporting ligand,[49-50] though the third expected component at higher fields was not observable (likely broad). Overall, it appears that spin isomerism is also present in this three-coordinate iron(III) hydrazido(2–) complex. Future studies will aim to unravel the reason why the 1:1 ratio is observed even without apparent crystal constraints.

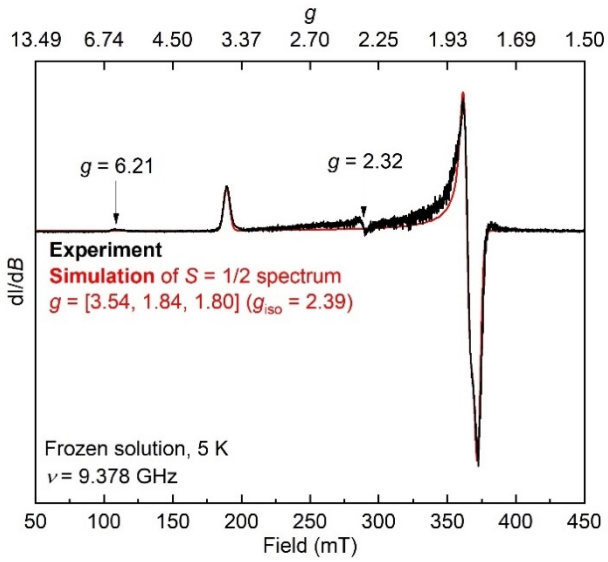

Figure 6. EPR spectrum of **8** in toluene at 5 K (black) and simulation of the $S = 1/2$ component (red).

Lastly, we explored the silylation of the iron(I) methyl complex **5c** (Scheme 5). Addition of bis(silyl) reagent **6** to a solution of **5c-N$_2$** in Et_2O at –116 °C led to an immediate color change from magenta to brown, which subsequently turned yellow upon warming to ambient temperature. The ^{1}H NMR spectrum of the crude reaction mixture showed the presence of two species: the oxidized iron(II) complex **4c** (57%) and a new C_s symmetric species **10** (37%). In this case, no **8** was observed in the crude mixture. X-ray crystallography identified **10** as a 1,2-bis(silyl)methylhydrazido complex (Figure 7). The quality of the X-ray diffraction data were too poor for quantitative structural information, but certainly show that the alkyl gives a different reaction outcome than the aryl migration previously described.[29] The frozen solution Mössbauer spectrum of **10** in cyclohexane at 80 K shows a doublet with parameters of $\delta = 0.92$ mm s^{-1} and $|\Delta E_Q| = 1.55$ mm s^{-1}, clearly indicating a high-spin iron(II) complex. Indeed, the solution magnetic moment of **10** is $\mu_{eff} = 5.1(2)\ \mu_B$, consistent with high-spin iron(II). One possible mechanism for the formation of **10** is through the initial formation of the formally iron(IV) complex **7c** followed

by methyl migration to form the expected methylhydrazido complex **11** (Scheme 5, bottom). This complex could then isomerize to give the observed product **10**. Isomerization of the bis(silyl)methylhydrazido ligand in the proposed complex **11** has precedent in the isomerization of free bis(trimethylsilyl)methylhydrazine in the presence of catalytic amounts of base.[51]

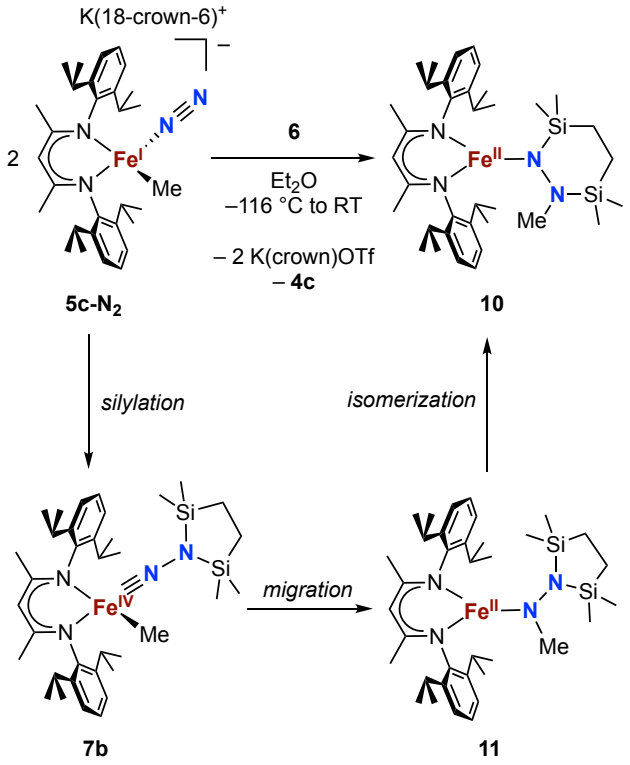

Scheme 5. Synthesis of the methylhydrazido complex **10**, and proposed mechanism of formation.

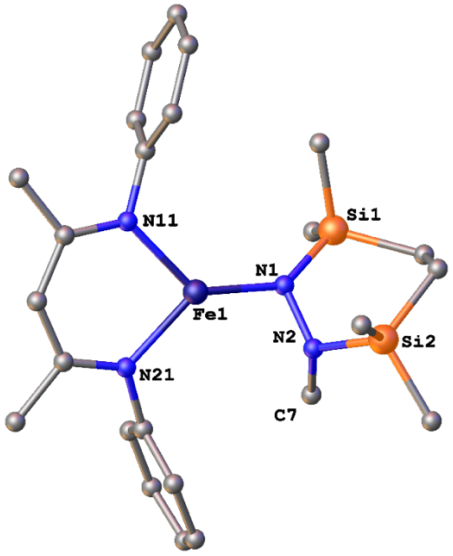

Figure 7. Ball-and-stick diagram of the connectivity structure of the methylhydrazido complex **10**. H atoms and ^{i}Pr groups omitted for clarity.

To determine whether the silyl migration arises from the change from trimethylsilyl to the bis(silyl) reagent **6**, the the iron(I) phenyl complex **1-N$_2$** was silylated with **6 (**Scheme 6).[29] This led to the expected 1,1-bis(silyl)phenylhydrazido complex **12** (Figure 8) without the unusual silyl shift observed in the methyl system. It is unclear whether the lack of isomerization by **12** to give the 1,2-bis(silyl)phenylhydrazido complex is the result of a high kinetic barrier or a thermodynamically unfavorable reaction. Regardless, this result suggests that the use of the bis(silyl) reagent is not the sole reason for hydrazido isomerization, and that the identity of the migrating hydrocarbyl ligand has some effect on the hydrazido isomerization.

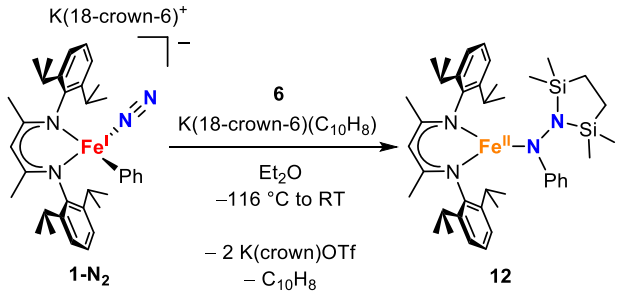

Scheme 6. Synthesis of the phenyl-migrated complex **12**.

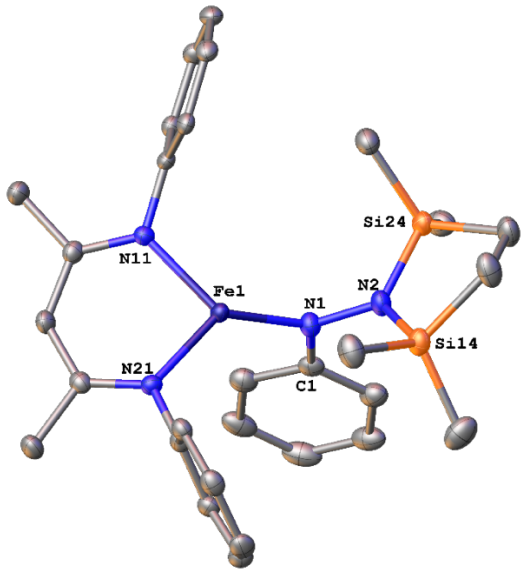

Figure 8. ORTEP diagram of **12** with thermal ellipsoids shown at 50% probability. H atoms and ^{i}Pr groups omitted for clarity.

The difference in product speciation between the silylation reactions of the benzyl complex **5b** and the methyl complex **5c** suggests that there may be two competing reaction pathways upon formation of the resulting formally iron(IV) alkyl complexes. These two competing reaction pathways were investigated using DFT calculations (Figure 9). Geometries were optimized using B3LYP/def2-TZVP in both the triplet and quintet states to probe possible spin-crossover behavior as observed in the aryl migration mechanism.[38]

No transition states were found for the Fe–C_{alkyl} bond homolysis steps in both the benzyl and methyl systems. Bond homolysis reactions typically have very low barriers,[52] and thus we assumed that Fe–C_{alkyl} bond homolysis is not slowed by any activation barrier. The quintet surface was calculated to be the lowest energy pathway for Fe–C homolysis in both systems. The barrier for Fe–C bond homolysis from the proposed iron(IV) *benzyl* complex **7b** is only 7 kcal mol^{-1}. Meanwhile, the barrier for Fe–C bond homolysis from the iron(IV) *methyl* complex is higher at 19 kcal mol^{-1}, likely stemming from the greater stability of a benzyl radical relative to a methyl radical (assuming the Hammond Postulate).[53]

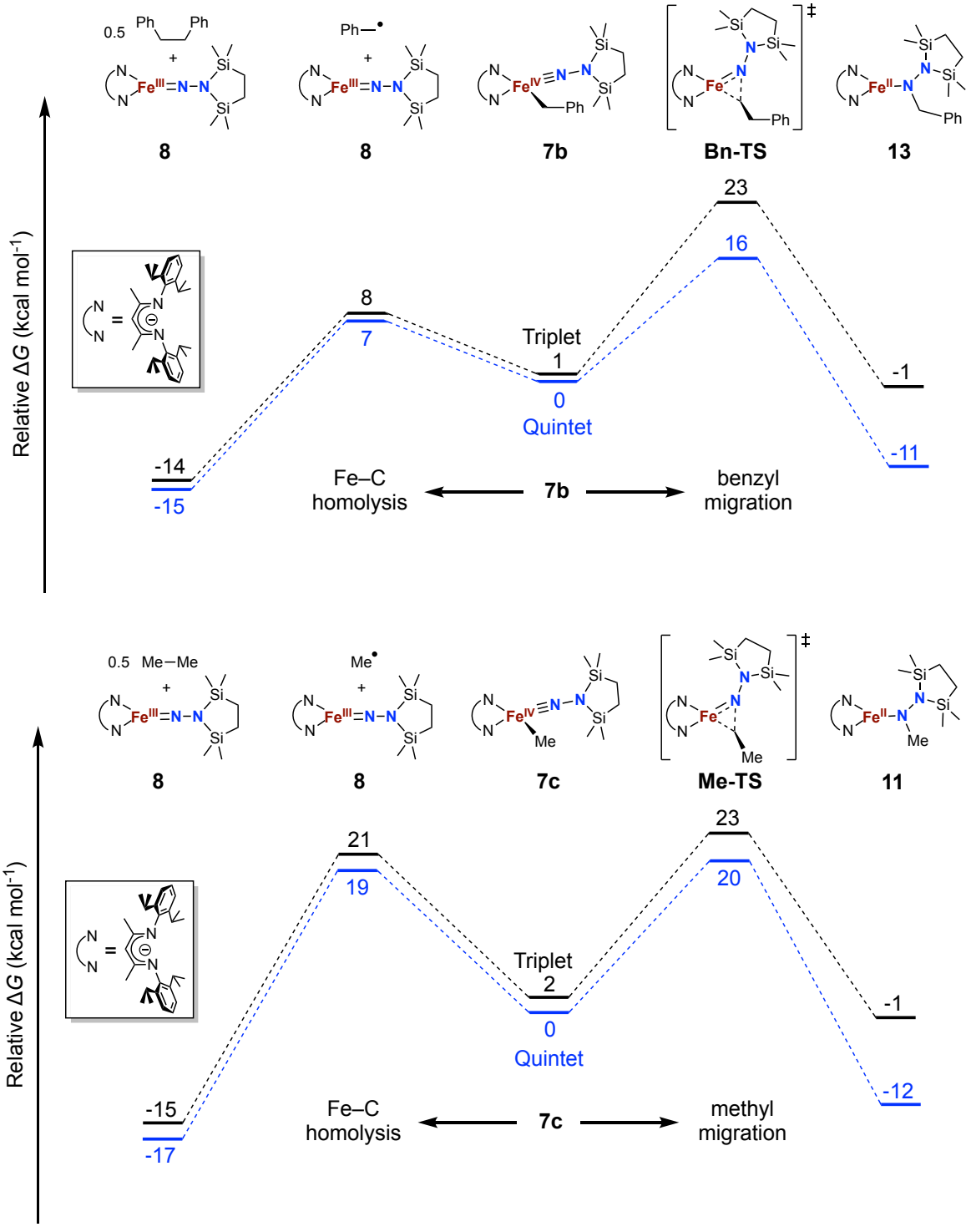

Figure 9. Potential energy surfaces of Fe–C bond homolysis (to the left) versus alkyl migration (to the right) starting from the proposed iron(IV) benzyl (top) and methyl (bottom) complexes from DFT calculations (B3LYP/def2-TZVP).

For the alkyl migration steps, the nudged-elastic band (NEB) method was used to find initial starting geometries for the transition states, which were then further optimized. Again, the lowest energy pathway was found on the quintet surface for both benzyl and methyl migration. The calculated barriers for benzyl (16 kcal mol^{-1}) and methyl (20 kcal mol^{-1}) migration are similar to the measured barriers of aryl migration (21–23 kcal mol^{-1}).[38]

The significantly lower barrier for Fe–C_{Bn} bond homolysis compared to that for benzyl migration is consistent with the observation that silylation of **5b-N_2** gave homolysis to the iron(III) complex **8** rather than migration. Meanwhile, the barrier for Fe–C_{Me} bond homolysis starting from **7c** is nearly identical to the barrier for methyl migration, suggesting that both reaction pathways may be occurring in the silylation reaction of **5c-N_2**. Alternatively, it may be possible that radical recombination after Fe–C_{Me} bond homolysis between the produced methyl radical and **8** could form the methyl migrated complex **11** in a two-step migration mechanism rather than a concerted migratory insertion step. A similar radical recombination mechanism has been proposed for migratory insertion of alkyl ligands into CO in iron(III) porphyrin complexes.[20] Nonetheless, these calculations suggest that for formally iron(IV) alkyl hydrazido(2–) complexes, Fe–C bond homolysis and alkyl migration can both be kinetically competitive reaction pathways.

Conclusions

In summary, we have shown that silylation of iron(I) alkyl N_2 complexes can give formally iron(IV) alkyl hydrazido(2–) species. With trimethylsilylmethyl, this product has a high-spin ground state in contrast to the previously isolated intermediate-spin iron(IV) phenyl analogue. Upon formation of the iron(IV) alkyl species, Fe–C bond homolysis as well as alkyl group migration can occur, with product speciation dependent on the alkyl ligand. DFT calculations

support the observed reactivities and show that both reaction pathways can be kinetically competitive at room temperature.

Importantly, we demonstrate that the use of formally iron(IV) centers leads to the formation of N–C_{akyl} as well as N–C_{aryl} bonds, showing the generalizability of this novel approach. However, the migration of alkyl ligands is problematic when the alkyl radical is stable enough for Fe–C bond homolysis to have a relatively low barrier. Thus, while alkyl migration was feasible for N–C bond formation to N_2, the selectivity of the reaction is poorer than the analogous aryl migration.

Acknowledgments

This research was supported by the U.S. Department of Energy, Office of Science, Office of Basic Energy Sciences, Catalysis Science program, under Award DE-SC0020315. We thank the Yale Center for Research Computing for guidance and use of the research computing infrastructure.

References

(1) Nam, W. *Acc. Chem. Res.* **2007,** *40*, 522-531.

(2) Scepaniak, J. J.; Margarit, C. G.; Harvey, J. N.; Smith, J. M. *Inorg. Chem.* **2011,** *50*, 9508-9517.

(3) Smith, J. M.; Subedi, D. *Dalton Trans.* **2012,** *41*, 1423-1429.

(4) Cramer, S. A.; Hernández Sánchez, R.; Brakhage, D. F.; Jenkins, D. M. *Chem. Commun.* **2014,** *50*, 13967-13970.

(5) Lee, W.-T.; Juarez, R. A.; Scepaniak, J. J.; Muñoz, S. B.; Dickie, D. A.; Wang, H.; Smith, J. M. *Inorg. Chem.* **2014,** *53*, 8425-8430.

(6) Muñoz, S. B.; Lee, W.-T.; Dickie, D. A.; Scepaniak, J. J.; Subedi, D.; Pink, M.; Johnson, M. D.; Smith, J. M. *Angew. Chem., Int. Ed.* **2015,** *54*, 10600-10603.

(7) Maity, A. K.; Murillo, J.; Metta-Magaña, A. J.; Pinter, B.; Fortier, S. *J. Am. Chem. Soc.* **2017,** *139*, 15691-15700.

(8) Golovanov, I. S.; Leonov, A. V.; Lesnikov, V. K.; Pospelov, E. V.; Frolov, K. V.; Korlyukov, A. A.; Nelyubina, Y. V.; Novikov, V. V.; Sukhorukov, A. Y. *Dalton Trans.* **2022,** *51*, 4284-4296.

(9) Lucas, R. L.; Powell, D. R.; Borovik, A. S. *J. Am. Chem. Soc.* **2005,** *127*, 11596-11597.

(10) Kumar, S.; Faponle, A. S.; Barman, P.; Vardhaman, A. K.; Sastri, C. V.; Kumar, D.; de Visser, S. P. *J. Am. Chem. Soc.* **2014,** *136*, 17102-17115.

(11) Wang, L.; Hu, L.; Zhang, H.; Chen, H.; Deng, L. *J. Am. Chem. Soc.* **2015,** *137*, 14196-14207.

(12) Mondal, B.; Roy, L.; Neese, F.; Ye, S. *Isr. J. Chem.* **2016,** *56*, 763-772.

(13) Lee, J. L.; Ross, D. L.; Barman, S. K.; Ziller, J. W.; Borovik, A. S. *Inorg. Chem.* **2021,** *60*, 13759-13783.

(14) Mansuy, D.; Battioni, J. P.; Dupre, D.; Sartori, E.; Chottard, G. *J. Am. Chem. Soc.* **1982,** *104*, 6159-6161.

(15) Casitas, A.; Rees, J. A.; Goddard, R.; Bill, E.; DeBeer, S.; Fürstner, A. *Angew. Chem., Int. Ed.* **2017,** *56*, 10108-10113.

(16) Jacobs, B. P.; Wolczanski, P. T.; Jiang, Q.; Cundari, T. R.; MacMillan, S. N. *J. Am. Chem. Soc.* **2017,** *139*, 12145-12148.

(17) Caulfield, K. P.; Tonzetich, Z. J. *Organometallics* **2022,** *41*, 155-160.

(18) Bower, B. K.; Tennent, H. G. *J. Am. Chem. Soc.* **1972,** *94*, 2512-2514.

(19) Lewis, R. A.; Smiles, D. E.; Darmon, J. M.; Stieber, S. C. E.; Wu, G.; Hayton, T. W. *Inorg. Chem.* **2013,** *52*, 8218-8227.

(20) Arafa, I. M.; Shin, K.; Goff, H. M. *J. Am. Chem. Soc.* **1988,** *110*, 5228-5229.

(21) Li, Z.; Goff, H. M. *Inorg. Chem.* **1992,** *31*, 1547-1548.

(22) Balch, A. L.; Olmstead, M. M.; Safari, N.; St. Claire, T. N. *Inorg. Chem.* **1994,** *33*, 2815-2822.

(23) Byungho, S.; Goff, H. M. *Inorg. Chim. Acta* **1994,** *226*, 231-235.

(24) Song, B.; Goff, H. M. *Inorg. Chem.* **1994,** *33*, 5979-5980.

(25) Riordan, C. G.; Halpern, J. *Inorg. Chim. Acta* **1996,** *243*, 19-24.

(26) Matsunaga, P. T.; Hess, C. R.; Hillhouse, G. L. *J. Am. Chem. Soc.* **1994,** *116*, 3665-3666.

(27) Koo, K.; Hillhouse, G. L. *Organometallics* **1996,** *15*, 2669-2671.

(28) Hu, X.; Meyer, K. *J. Am. Chem. Soc.* **2004,** *126*, 16322-16323.

(29) McWilliams, S. F.; Broere, D. L. J.; Halliday, C. J. V.; Bhutto, S. M.; Mercado, B. Q.; Holland, P. L. *Nature* **2020,** *584*, 221-226.

(30) Nagelski, A. L.; Fataftah, M. S.; Bollmeyer, M. M.; McWilliams, S. F.; MacMillan, S. N.; Mercado, B. Q.; Lancaster, K. M.; Holland, P. L. *Chem. Sci.* **2020,** *11*, 12710-12720.

(31) Deegan, M. M.; Peters, J. C. *Chem. Sci.* **2018,** *9*, 6264-6270.

(32) Smith, J. M.; Lachicotte, R. J.; Holland, P. L. *Organometallics* **2002,** *21*, 4808-4814.

(33) Vela, J.; Vaddadi, S.; Cundari, T. R.; Smith, J. M.; Gregory, E. A.; Lachicotte, R. J.; Flaschenriem, C. J.; Holland, P. L. *Organometallics* **2004,** *23*, 5226-5239.

(34) Sciarone, T. J. J.; Meetsma, A.; Hessen, B. *Inorg. Chim. Acta* **2006,** *359*, 1815-1825.

(35) MacLeod, K. C.; DiMucci, I. M.; Zovinka, E. P.; McWilliams, S. F.; Mercado, B. Q.; Lancaster, K. M.; Holland, P. L. *Organometallics* **2019,** *38*, 4224-4232.

(36) Moret, M.-E.; Peters, J. C. *J. Am. Chem. Soc.* **2011,** *133*, 18118-18121.

(37) Rudd, P. A.; Planas, N.; Bill, E.; Gagliardi, L.; Lu, C. C. *Eur. J. Inorg. Chem.* **2013,** *2013*, 3898-3906.

(38) Bhutto, S. M.; Hooper, R. X.; Mercado, B. Q.; Holland, P. L. *ChemRxiv* **2022**.

(39) Hoffmann, R.; Alvarez, S.; Mealli, C.; Falceto, A.; Cahill, T. J.; Zeng, T.; Manca, G. *Chem. Rev.* **2016,** *116*, 8173-8192.

(40) Piascik, A. D.; Li, R.; Wilkinson, H. J.; Green, J. C.; Ashley, A. E. *J. Am. Chem. Soc.* **2018,** *140*, 10691-10694.

(41) McWilliams, S. F.; Bill, E.; Lukat-Rodgers, G.; Rodgers, K. R.; Mercado, B. Q.; Holland, P. L. *J. Am. Chem. Soc.* **2018,** *140*, 8586-8598.

(42) Caulfield, K. P.; Conradie, J.; Arman, H. D.; Ghosh, A.; Tonzetich, Z. J. *Inorg. Chem.* **2019,** *58*, 15225-15235.

(43) Kim, D.; Rahaman, S. M. W.; Mercado, B. Q.; Poli, R.; Holland, P. L. *J. Am. Chem. Soc.* **2019,** *141*, 7473-7485.

(44) Barroso, S.; Coelho, A. M.; Adão, P.; Calhorda, M. J.; Martins, A. M. *Dalton Trans.* **2017,** *46*, 9692-9704.

(45) McWilliams, S. F.; Bill, E.; Lukat-Rodgers, G.; Rodgers, K. R.; Mercado, B. Q.; Holland, P. L. *J. Am. Chem. Soc.* **2018,** *140*, 8586-8598.

(46) Cowley, R. E.; DeYonker, N. J.; Eckert, N. A.; Cundari, T. R.; DeBeer, S.; Bill, E.; Ottenwaelder, X.; Flaschenriem, C.; Holland, P. L. *Inorg. Chem.* **2010,** *49*, 6172-6187.

(47) Paulsen, H.; Trautwein, A. X., Density Functional Theory Calculations for Spin Crossover Complexes. In *Spin Crossover in Transition Metal Compounds III*, Gütlich, P.; Goodwin, H. A., Eds. Springer Berlin Heidelberg: Berlin, Heidelberg, 2004; pp 197-219.

(48) McWilliams, S. F.; Brennan-Wydra, E.; MacLeod, K. C.; Holland, P. L. *ACS Omega* **2017,** *2*, 2594-2606.

(49) Cowley, R. E.; Eckert, N. A.; Elhaïk, J.; Holland, P. L. *Chem. Commun.* **2009**, 1760-1762.

(50) Eckert, N. A.; Vaddadi, S.; Stoian, S.; Lachicotte, R. J.; Cundari, T. R.; Holland, P. L. *Angew. Chem., Int. Ed.* **2006,** *45*, 6868-6871.

(51) West, R.; Ishikawa, M.; Bailey, R. E. *J. Am. Chem. Soc.* **1967,** *89*, 4068-4072.

(52) Poli, R. *Comptes Rendus. Chimie* **2021,** *24*, 147-175.

(53) Hammond, G. S. *J. Am. Chem. Soc.* **1955,** *77*, 334-338.